10.1098/rsta.2004.1442

THE ROYAL SOCIETY

Raman scattering of non-planar graphite: arched edges, polyhedral crystals, whiskers and cones

By PingHeng Tan[1], Svetlana Dimovski[2] and Yury Gogotsi[2]

[1]*State Key Laboratory for Superlattices and Microstructures, Institute of Semiconductors, Chinese Academy of Sciences, Beijing 100083, People's Republic of China*

[2]*Department of Materials Science and Engineering and A. J. Drexel Nanotechnology Institute, Drexel University, Philadelphia, PA 19104, USA* (gogotsi@drexel.edu)

Planar graphite has been extensively studied by Raman scattering for years. A comparative Raman study of several different and less common non-planar graphitic materials is given here. New kinds of graphite whiskers and tubular graphite cones (synthetic and natural) have been introduced. Raman spectroscopy has been applied to the characterization of natural graphite crystal edge planes, an individual graphite whisker, graphite polyhedral crystals and tubular graphite cones. Almost all of the observed Raman modes were assigned according to the selection rules and the double-resonance Raman mechanism. The polarization properties related to the structural features, the line shape of the first-order dispersive mode and its combination modes, the frequency variation of some modes in different carbon materials and other unique Raman spectral features are discussed here in detail.

Keywords: Raman scattering; non-planar graphite; arched edge; polyhedral crystal; whisker; cone

1. Introduction

Raman spectroscopy, because of its sensitivity to changes in the atomic structure of carbons, has proved helpful in understanding the vibration properties and the microstructure of graphitic crystals and various disordered graphite materials (Tuinstra & Koenig 1970; Vidano & Fischbach 1978; Lespade *et al*. 1982; Dillon *et al*. 1984; Katagiri *et al*. 1988; Nemanich *et al*. 1988; Kawashima & Katagiri 1995; Dresselhaus *et al*. 1999). The relation between the spectra and the structure has been extensively discussed in the literature and the studies cover a wide range of carbon materials, such as (ion-implanted) highly oriented pyrolytic graphite (HOPG) (Nemanich & Solin 1979; Kawashima & Katagiri 1995; Tan *et al*. 1998), pyrolytic graphite (PG) (Katagiri *et al*. 1988; Kawashima & Katagiri 1995), microcrystalline graphite, amorphous and glassy carbon, fullerenes, carbon onions, nanotubes, etc.

One contribution of 13 to a Theme 'Raman spectroscopy in carbons: from nanotubes to diamond'.

In addition to the above materials, some non-planar graphitic structures have been synthesized or found in nature (Jaszczak 1995; Dimovski *et al*. 2004; Jaszczak *et al*. 2003) during the past few years. They include graphite polyhedral crystals, tubular graphite cones, carbon cones and graphitic whiskers. Some of those structures had been first reported decades ago (Haanstra *et al*. 1972) and recently rediscovered, when interest in carbon nanotubes attracted hundreds of scientists to this area. For example, a new type of graphite whisker had been synthesized in a graphitization furnace using a high-temperature heat-treatment method at a special pressure (Dong *et al*. 2001). The so-called tubular graphite cone (TGC) is also synthesized on an iron needle using a chemical vapour deposition method (Zhang *et al*. 2003). Graphite polyhedral crystals (GPCs) (Gogotsi *et al*. 2000) and small-apex-angle graphite conical crystals (GCCs) (Dimovski *et al*. 2002; Gogotsi *et al*. 2002) have been recently reported to form in the pores of glassy carbon at high temperatures. The diameters of the whiskers and the cone roots can reach up to 1 μm, and their lengths can reach up to 20 μm. Graphite conical and polyhedral crystals from glassy carbon pores usually do not exceed 300 and 1000 nm in diameter, respectively, and their lengths are up to several micrometres. The size and aspect ratio of such non-planar graphitic crystals enable acquisition of Raman spectra from the individual crystals. However, the Raman spectra of these non-planar graphitic structures have never been reviewed or analysed in detail. In the following, we will briefly describe the structure of graphite polyhedral crystals, graphite whiskers and graphitic cones, and then review the Raman scattering from an individual graphite polyhedral crystal (Gogotsi *et al*. 2000), graphite whisker (Tan *et al*. 2001, 2002), tubular graphite cone (Tan *et al*. 2004) and other non-planar graphitic crystals. Since the surfaces of the majority of the axial graphitic structures described here are dominated by edges, not by graphitic basal planes, we find it appropriate to review the Raman scattering from graphite edge planes in the next section.

2. Raman scattering from a natural graphite crystal edge planes

Raman scattering from planar graphite has been studied extensively; however, most of the reported studies have been conducted on graphite basal plane (Tuinstra & Koenig 1970; Nemanich & Solin 1979; Lespade *et al*. 1982), while only a few studies deal with graphite edge planes (Katagiri *et al*. 1988; Bowling *et al*. 1989; Compagnini *et al*. 1997; Kawashima & Katagiri 1999). Moreover, almost all of the published studies were performed on the edge planes of HOPG, while there were no Raman spectra reported for the natural graphite edge planes. We studied Raman scattering from pristine natural graphite edge planes (Crestmore graphite), as seen in figure 1. Because of their softness and flexibility, quality natural graphite crystals may be rarer than diamonds. Due to the atomic crystal structure, the symmetry and the nature of the bonding, the growth of the graphite crystals is typically fastest at the edges in the direction parallel to the basal plane and perpendicular to prismatic crystal faces. As a result, the tabular hexagonal plates (figure 1*a*) are found to be the typical morphology of graphite crystals (Jaszczak 1995).

The first- and second-order Raman spectra from the isolated Crestmore graphite hexagonal plate for three different laser excitations (514.5 nm, 633 nm and 780 nm) are given in figure 2. The Raman measurements were conducted on the graphite basal plane, and the edge planes with the incident light polarized parallel and perpendicular

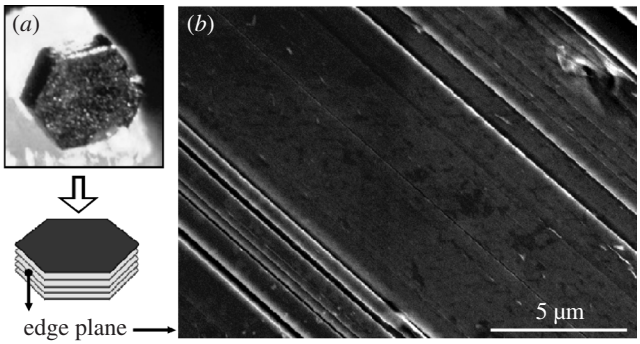

Figure 1. Well-formed natural graphite crystal (1.3 mm wide) occurring in a limestone from the Crestmore quarries, CA. (*a*) An optical micrograph of the crystal partly embedded in the limestone matrix. The basal plane exhibits numerous etch pits. (*b*) A scanning electron microscope (SEM) image showing a detail of the graphite edge plane from the prismatic face of the same crystal.

to the basal plane. Solid lines denote the spectra after baseline correction. The first-order region of the Raman spectra of the edge plane shows a strong and narrow graphitic 1582 cm^{-1} line with a full-width half-maximum (FWHM) of 14.5 cm^{-1}, as well as the two additional features at *ca.* 1360 and 1620 cm^{-1} (figure 2*a*). Intensities of the *ca.* 1360 and 1620 cm^{-1} bands change with the edge orientation with respect to the laser polarization plane. A careful examination shows that these two bands actually consist of the two subbands each (*ca.* 1352 and *ca.* 1369, and *ca.* 1620 and *ca.* 1624 cm^{-1} in the case of 514.5 nm excitation), as shown in figure 3. The second-order Raman spectra exhibit three distinct energy dispersive features at *ca.* 2440, *ca.* 2727 and *ca.* 3248 cm^{-1} (figure 2*a*) and an additional low-intensity narrow line at *ca.* 2328 cm^{-1} (figure 2*b*). Several other fundamental modes have been observed in the first-order Raman spectra region (1113, 1242, 1495 and 1650 cm^{-1} bands with 633 nm excitation; 1084, 1148, 1198 and 1488 cm^{-1} bands with 780 nm), as well as energy dispersive 1745–1787 and 1950 cm^{-1} overtones.

A single crystal of graphite belongs to the D^4_{6h} symmetry group; the irreducible representation for the Brillouin zone (BZ) centre optical modes can be decomposed into

$$\Gamma = A_{2u} + 2B_{2g} + E_{1u} + 2E_{2g}. \tag{2.1}$$

Only the $2E_{2g}$ modes are Raman active, and they have been observed at 42 and 1582 (G) cm^{-1}, respectively (Nemanich & Solin 1979). Infrared-active A_{2u} and E_{1u} modes have been observed at 867.8 and 1588 cm^{-1} (Nemanich *et al.* 1977), and one of the two optically inactive B_{2g} modes has been found at 127 cm^{-1} by neutron scattering (Nicklow *et al.* 1972). The other B_{2g} mode that corresponds to 'out-of-plane' atomic displacements was reported in a Raman spectrum of HOPG edge planes by Kawashima & Katagiri (1999). The peak presence is possible when the Raman inactive B_{2g} mode becomes Raman active by modification of crystalline point group symmetry due to a slight rearrangement of lattice structure at the vicinity of the edge (Kawashima & Katagiri 1999). As a consequence, a sharp peak is observed at 864 cm^{-1} for the 633 nm laser excitation (figure 2*b*) and 863 cm^{-1} in the case of 780 nm laser excitation (figure 2*c*) when the incident light is polarized perpendic-

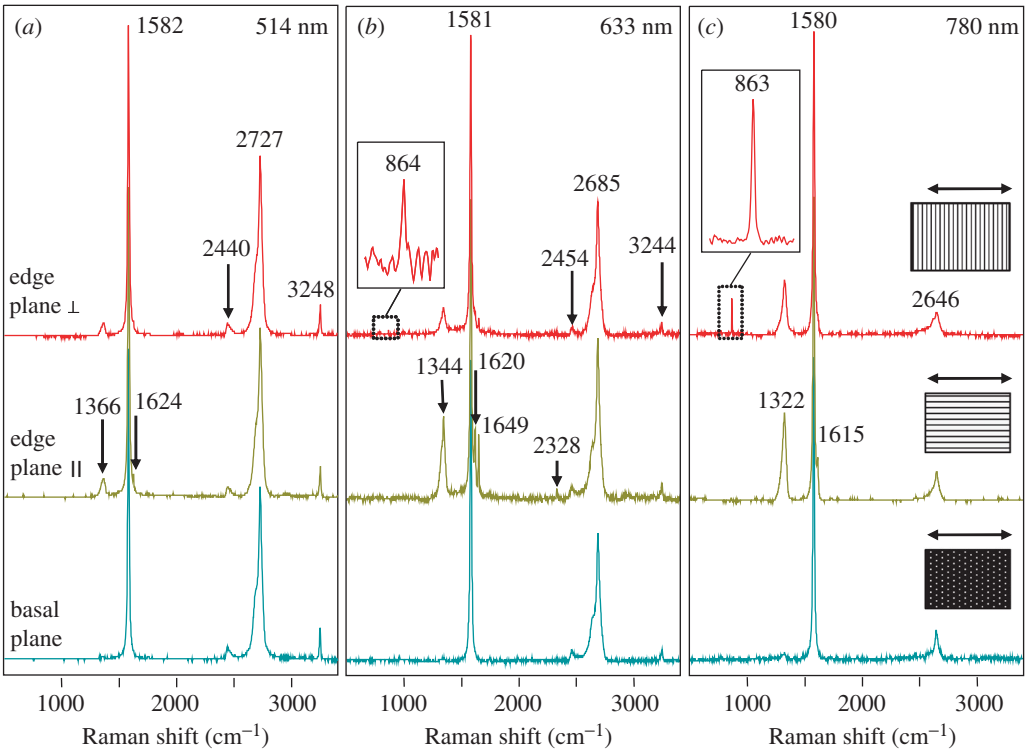

Figure 2. First- and second-order Raman spectra of graphite crystal basal and edge planes as a function of incident beam energy and edge orientation with respect to polarized beam.

ular to the basal plane. 'Out-of-plane' related peak positions for the higher-energy excitations were reported as well (Kawashima & Katagiri 1999).

In addition to the $k = 0$ zone-centre modes, several other bands are observed that can be attributed to $k \neq 0$ Raman forbidden fundamental modes (figure 2). The two first-order lines at *ca.* 1360 (D) cm^{-1} and *ca.* 1620 (D′) cm^{-1} (excited with 514.5 nm laser light) have been reported for microcrystalline graphite (Nemanich & Solin 1979), pristine HOPG (Tan *et al.* 1998) and ion-implanted HOPG (Compagnini *et al.* 1997). Furthermore, the D and D′ bands have also been observed in the Raman spectrum of graphite edge planes (Katagiri *et al.* 1988) and in the inner/outer surfaces of shortened cup-stacked-type carbon nanotubes (Endo *et al.* 2003). Such Raman forbidden bands ($k \neq 0$) become Raman active due to the double-resonance (DR) Raman mechanism. For the DR process in graphite (Thomsen & Reich 2000; Saito *et al.* 2002), an electron with momentum k (and electron energy $E^{\mathrm{i}}(k)$) is excited by the incident laser photon in an electron–hole creation process. The electron is then scattered by emitting or absorbing a phonon with momentum q to the state with momentum $k+q$ (and energy $E(k+q)$), then scattered again back to the state with momentum k (and electron energy $E^{\mathrm{f}}(k)$) to recombine with a hole. In general, there exist four possible DR scattering processes for the Stokes and anti-Stokes Raman scatterings (Saito *et al.* 2002). The phonon wave vector q of the phonon mode $\omega(q)$ involved in each resonance process is determined from the two resonant electronic states by the energy-momentum conservation condition. The D mode is

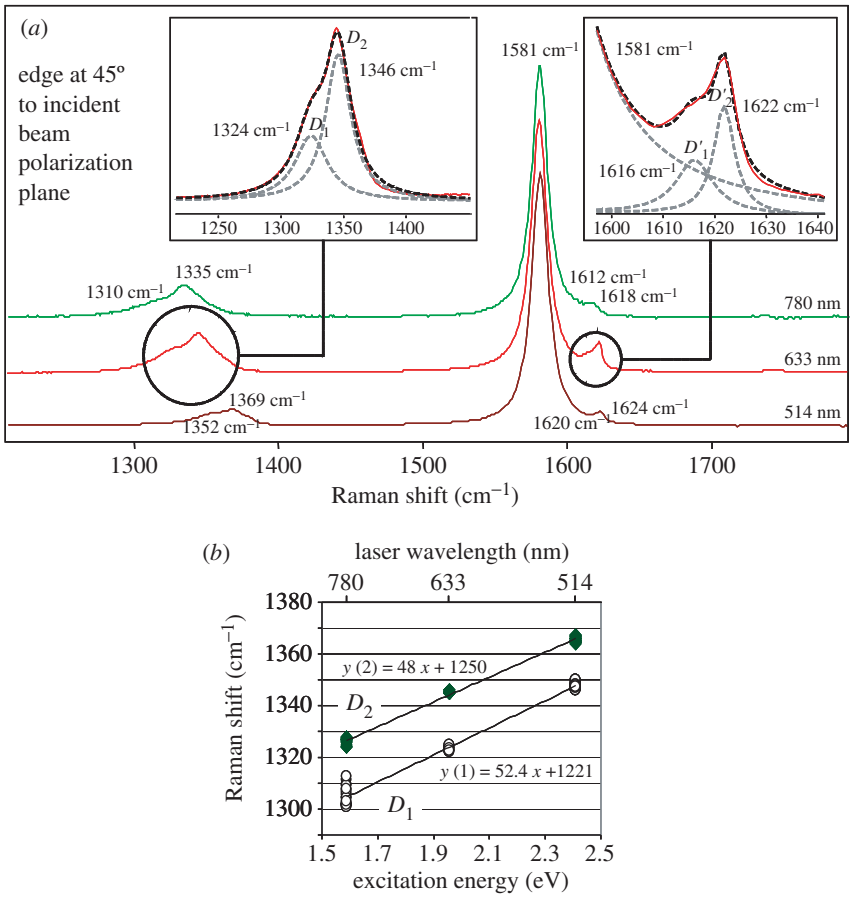

Figure 3. (*a*) Doublets of D (D_1 and D_2) and D′ (D'_1 and D'_2) bands for three different excitation wavelengths. (*b*) Frequency of D_1 and D_2 bands as a function of laser excitation energy.

explained by an inter-valley DR mechanism that occurs around two inequivalent K points at neighbouring corners of the first BZ, while the D′, L_1 and L_2 modes can be explained by an intra-valley DR mechanism that occurs around the K point in the BZ of graphite (Saito *et al*. 2002; Grüneis *et al*. 2002; Cançado *et al*. 2002; Tan *et al*. 2002). The inter-valley and intra-valley DR mechanisms also successfully explain the spectral behaviours of the Stokes and anti-Stokes lines of the second-order Raman modes in graphite materials (Cançado *et al*. 2002; Tan *et al*. 2002; Brar *et al*. 2002), as discussed in the following text.

Figure 3*a* shows Raman spectra of the crystal edge plane with clear doublets of D and D′ bands. A lower-energy shoulder (D_1) is found at 1352 cm^{-1} and a higher-energy shoulder (D_2) at 1369 cm^{-1} (excited with 514.5 nm light). The intensity of the D_2 band (relative to the G band) shows a drastic dependence on edge orientation (figure 2) and is generally higher when the incident beam polarization plane is parallel to the edge plane of the sample. Such behaviour was not observed for the D_1 band. Both the D_1 and D_2 lines are energy dispersive (figure 3), and the slopes $\partial\omega_1/\partial E$ and $\partial\omega_2/\partial E$ are both close to 50 cm^{-1} eV^{-1} (figure 3*b*). The D band doublet at *ca.* 1360 cm^{-1} (or *ca.* 1355 cm^{-1}) has already been reported in the Raman spectra of

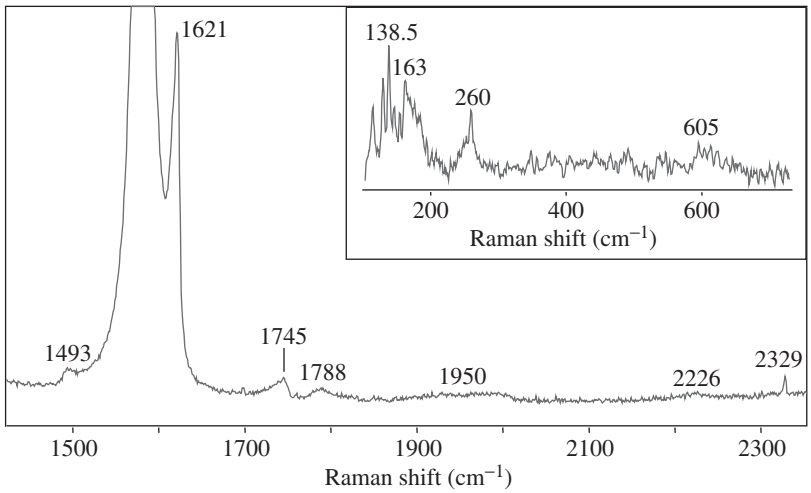

Figure 4. Raman spectrum from graphite crystal edge plane in the 1700–2300 cm^{-1} region (633 nm excitation, polarized incident and scattered light). Inset shows low-frequency lines.

ion-implanted HOPG samples (Compagnini *et al*. 1997; Tan *et al*. 1998). Compagnini *et al*. (1997) observed the differences between the two shoulders of the D band. They noted that the lower-energy shoulder is a typical feature of the edge plane Raman spectra, while the upper-energy peak depends on the number of defects introduced and is a disorder-related band. Because the frequency splitting of the D_1 and D_2 lines of the crystal edge plane is similar to that of the doublet in ion-implanted HOPG, the physical origin of these two peaks may be related to the coupling between the A and B graphene layers that are stacked in the highly ordered $\cdots$ABAB$\cdots$ structure (Tan *et al*. 1999; Ferrari & Robertson 2000). The doublets in figure 3 are not related to the doublets observed in two-dimensional graphite (Cançado *et al*. 2002) and whiskers (figure 9) whose frequency splitting is *ca*. 9 cm^{-1} (a frequency difference between the Stokes and anti-Stokes components of the D mode). The D′ band doublet at *ca*. 1620 cm^{-1} is not always very distinct; however, the inset in figure 3*a* shows a Raman spectrum from the edge plane obtained with 633 nm excitation having a clearly asymmetric D′ feature. This *ca*. 1620 cm^{-1} band can be fitted with a lower- D'_1 and a higher- D'_2 energy shoulder at 1616 and 1622 cm^{-1} (with 633 nm excitation). As in the case of the D_2 line, the intensity of D'_2 also varies with the edge orientation and is generally stronger when the edge is parallel to the incident light polarization plane (figure 2).

Other prominent features in the Raman spectra of natural graphite crystal edge planes include a non-dispersive *ca*. 1750 cm^{-1} (M) band and *ca*. 1950 cm^{-1} energy-dispersive iTOLA feature (figure 4), but also some weak-intensity lines observed occasionally in the region of low-frequency values (figure 4, inset). The M band at 1750 cm^{-1} consists of two shoulders, 1745 and 1788 cm^{-1}, and it has been assigned to an overtone of the infrared-active 'out-of-plane' mode at *ca*. 864 cm^{-1} in graphite (Brar *et al*. 2002). The energy-dispersive mode at 1950 cm^{-1} is tentatively identified as a combination of the in-plane transverse optic (iTO) and longitudinal acoustic (LA) modes in the same reference. The reason for the presence of the low-frequency lines at *ca*. 138.5, 163 and 260 cm^{-1} is, however, unclear, but it may be due to

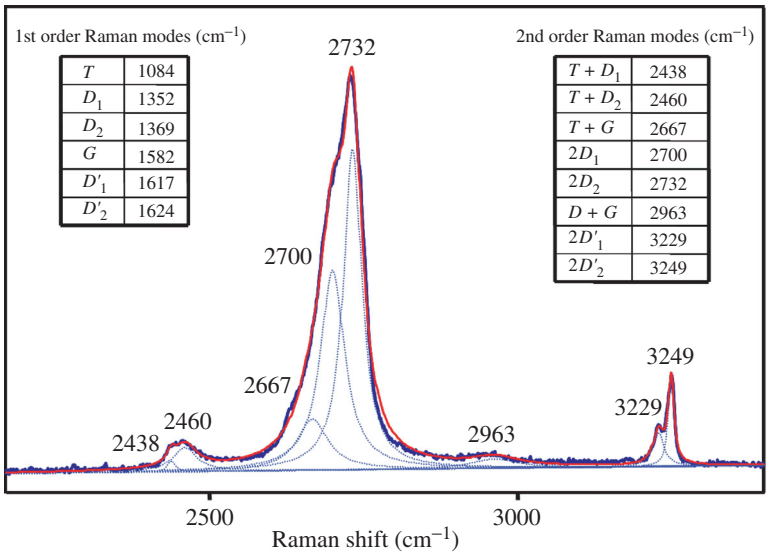

Figure 5. Second-order Raman spectrum from graphite crystal edge plane for 514.5 nm excitation (polarized incident and scattered light).

acoustic phonon branch modes that become Raman active by the intra-valley DR Raman process, as suggested by Saito *et al.* (2002) for graphite whisker low-frequency lines (Tan *et al.* 2001). Similarly, the feature at 1492 cm^{-1} can be assigned to the TO phonon branch (Saito *et al.* 2002).

The overtones and combination bands of natural graphite crystal edge planes are shown in figure 5. The second-order Raman spectra mainly comprise features (2438, 2460, 2700, 2732, 2963 and 3249 cm^{-1}) which have been described and assigned elsewhere in the literature (Tan *et al.* 1998). We observed a 2667 cm^{-1} (T + G) combination mode, and a highly pronounced lower-energy shoulder of a $2D'_2$ mode at 3229 cm^{-1} that is believed be the $2D'_1$ overtone. The splitting of the 2D and 2D′ bands is consistent with observations from the first-order spectra. The doublet (sometimes triplet) at *ca.* 3240 cm^{-1} has also been observed in Raman spectra of graphite polyhedral crystals, which will be described in detail in § 5. We tentatively assign the D'_1 feature to the brim (loop) edge structure of terminated graphite planes.

3. Raman scattering of an individual graphite whisker

There are many methods of producing graphite whiskers (Bacon 1960). Carbon layers in whiskers are usually parallel to the growth axes of graphite whiskers and their cross-sections are circular. By using iron catalysts in hydrocarbon atmospheres, one kind of ribbon-like graphite whisker can be synthesized at *ca.* 700 °C, in which the carbon layers are normal to the growth axes (Murayama & Maeda 1990). Conical spiral crystals of graphite can be prepared by heat treatment of carbon black (Tsuzuku 1957). Recently, another type of graphite whisker was synthesized in a graphitization furnace using a high-temperature heat-treatment method under a special pressure (Dong *et al.* 2001), where the raw material consisted of graphite particles ground in a planetary mill. Carbon layers in these whiskers are almost perpendicular to their growth axes and a spiral structure is formed around them, as shown in figure 6*a*.

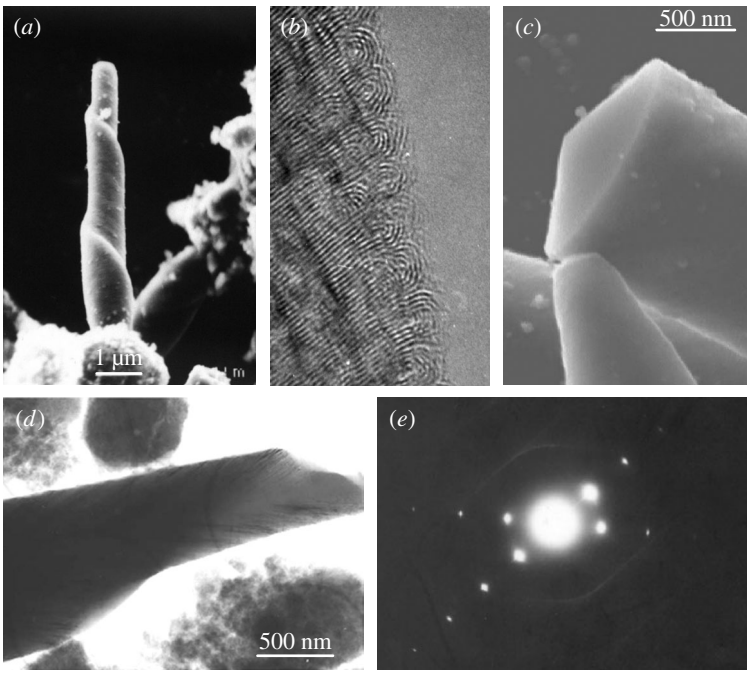

Figure 6. (*a*) SEM micrograph of a whisker. (*b*) High-resolution TEM micrograph corresponding to the right part of the tip in (*a*). (*c*) Fracture surface of a whisker with a conical shape, which proves that the whisker is composed of conical carbon layers. (*d*) A bright field image of a whisker tip. (*e*) The electron diffraction pattern in the region around a whisker axis.

The probability of observing clockwise versus anticlockwise spirals is almost equal in these structures. A typical lattice image of the brim region (figure 6*b*) shows a well-ordered graphitic structure. Figure 6*c* shows a circular cone at the tip of the whisker and the angle of its cone apex is *ca.* 133°, which means that the graphite whiskers are composed of a series of conical carbon layers with a conic angle of *ca.* 135°. The electron diffraction pattern (figure 6*e*) of the whisker axis confirms this assumption and reveals that this type of whisker is not formed by the spiral mechanism. Although spirals are observed on the whisker surface, whisker growth does not depend on the screw dislocation mechanism (Minkoff 1986). Further analysis on the transmission electron microscope (TEM) images and X-ray diffraction patterns of as-grown samples shows that the sample contains ZrC nanoparticles whose sizes range from 100 to 350 nm. During the ball-milling process of the carbon powder, the scrape breaks away from the zirconium oxide balls, mixes with carbonaceous materials, and becomes ZrC at high temperature. Carbon vapour deposits on the surface of ZrC nanoparticles at high temperature and forms whiskers with spirals by a disclination growth mechanism (Dong *et al*. 2003).

Because carbon layers in whiskers are usually parallel to the growth axes of graphite whiskers, it is expected that their Raman spectra are very similar to those of (disordered) graphite crystals and carbon fibres. Therefore, little work is carried out on the Raman scattering from graphite whiskers although Raman scattering from graphite crystals and their various disordered forms has been studied extensively. Their size, aspect ratio and unique structure allow for probing the material's

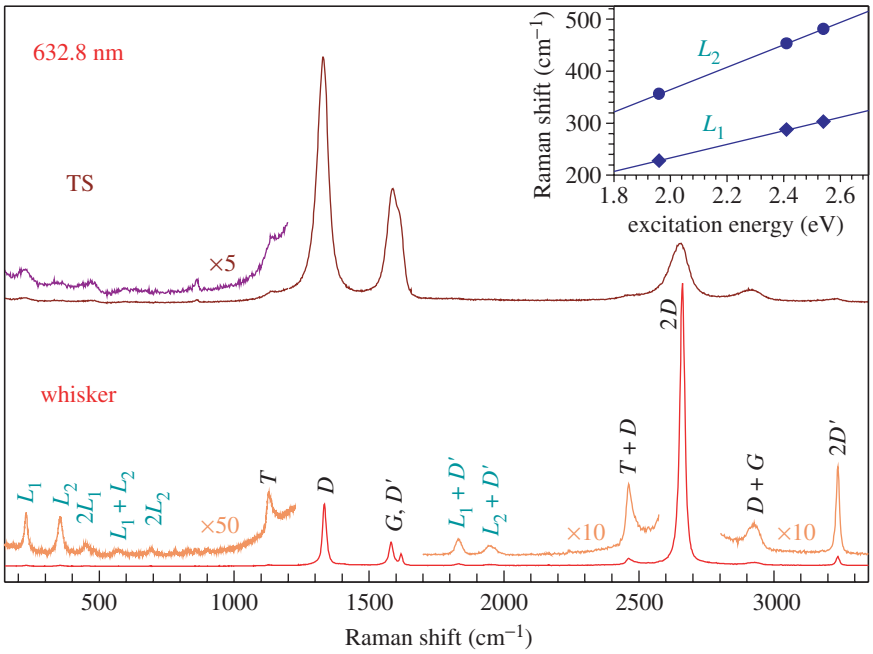

Figure 7. Raman spectra of TS structures and an individual graphite whisker excited with 632.8 nm laser excitation. The inset gives the energy dependence of the frequencies of the L_1 and L_2 modes.

vibrational properties from single whiskers and give an understanding of the phonon spectrum's dependence on the whisker structure.

Figure 7 shows the Raman spectra of an individual graphite whisker and turbostratically stacked (TS) particles using 632.8 nm excitation. Most first- and second-order Raman modes in whiskers and TS particles can be assigned to the corresponding modes in HOPG and PG (Kawashima & Katagiri 1995; Tan *et al*. 1998), such as the D, G and D′ modes at *ca*. 1333, 1582 and 1618 cm^{-1}, respectively.

In contrast to other carbon materials, the Raman spectra of whiskers exhibit several distinct characteristics. First, the intensity of the 2D overtone is found to be 13 times stronger than that of the first-order G mode in whiskers, while that of the 2D mode in TS particles is only one-fifth of the G mode. The strong enhancement of the D and 2D modes is also found in the Raman spectra of whiskers with 488.0 and 514.5 nm laser excitations, as shown in figure 8. Second, there are two additional low-frequency sharp peaks located at *ca*. 228 cm^{-1} and 355 cm^{-1}, and two additional strong modes (*ca*. 1833 and 1951 cm^{-1}) appeared at the second-order frequency region. Although the intensity ratio of the D mode to the G mode is up to 2.8, which is larger than that (2.3) of TS particles, many modes of whiskers still exhibit smaller line widths than those of TS particles. The line widths of the D, G, D′, 2D and 2D′ modes in whiskers (TS particles) are 17 (48), 18 (46), 10 (27), 20 (75) and 14 (70) cm^{-1}, respectively.

Besides the D and 2D modes, other dispersive modes, such as the T, D′, D + G and 2D′ modes in whiskers, also show a stronger relative intensity than the corresponding modes in TS particles, disordered graphite and carbon nanotubes for three laser excitations (Kawashima & Katagiri 1995; Tan *et al*. 1999). However, the intensity

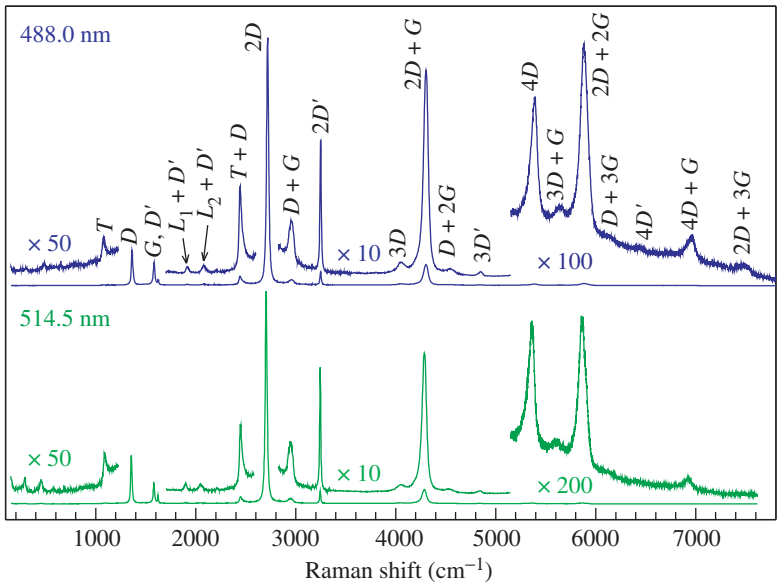

Figure 8. Raman spectra of an individual graphite whisker excited with 488.0 nm and 514.5 nm laser excitations.

of the G mode in whiskers is found to be equal to that in HOPG and does not exhibit any signs of intensity enhancement under the same experimental conditions. The intensity enhancement of the dispersive modes indicates that the DR Raman scattering may be responsible for this phenomenon. The fact that the layer-folded structures in the brim region of whiskers induce the coupled coherent electronic states between the neighbouring carbon layers may enhance the DR Raman effect for the dispersive modes in the new type of whisker. The intensity enhancement of the 2D mode is also observed in graphite polyhedral crystals (see figure 13) that have a similar structure in their brim regions (Gogotsi *et al.* 2000). Because of the intensity enhancement of the dispersive modes, the intensity ratio of the D band to the G band cannot be applied to the estimation of the degree of structural disorder for such carbon materials, although the crystallite planar size in disordered graphite was reported to be inversely proportional to the relative intensity of the D mode to the G mode (Tuinstra & Koenig 1970).

Compared with the Raman spectra of other carbon materials, graphite whiskers exhibit two intrinsic modes located at 228 cm^{-1} (L_1) and 355 cm^{-1} (L_2) for an excitation energy of $\varepsilon_{\mathrm{laser}} = 1.96$ eV, which are strongly dependent on the excitation energy with slopes of 129 and 216 $\mathrm{cm}^{-1}\,\mathrm{eV}^{-1}$ for the L_1 and L_2 modes, respectively (figure 7 inset). Because the frequencies of these two modes are in the frequency region of acoustic modes, the observed L_1 and L_2 modes were supposed to be the resonantly excited acoustic modes in the transverse-acoustic and longitudinal-acoustic phonon branches, which was confirmed by the recent theoretical model of the DR Raman process (Saito *et al.* 2002). The two modes with relatively lower phonon frequencies were also observed in multi-walled carbon nanotubes (Tan *et al.* 2002). According to the DR Raman process, the frequency of a combination mode is a little lower than the frequency sum of its two fundamentals in graphite materials (Tan *et al.* 2002), such a frequency of the $\mathrm{L}_1 + \mathrm{D}'$ mode in whiskers is *ca.* $-\frac{1}{2}\hbar\omega_{\mathrm{D}'} \times \partial\omega_{\mathrm{L}_1}/\partial\varepsilon_{\mathrm{laser}}$

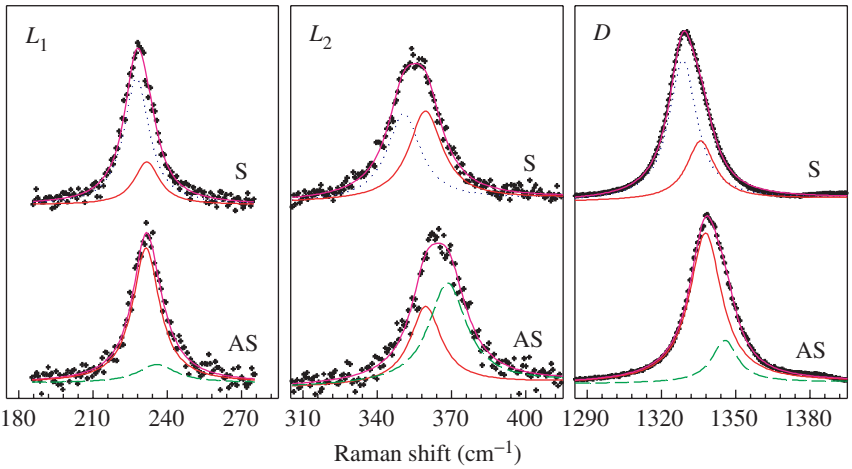

Figure 9. Stokes (S) and anti-Stokes (AS) Raman spectra of the L_1, L_2 and D modes in a graphite whisker excited with 632.8 nm laser excitation.

lower than the frequency sum of the L_1 and D′ modes. According to the frequency match, the two high-frequency modes at 1833 and 1951 cm^{-1} can be designated as $L_1 + D'$ and $L_2 + D'$ modes, respectively. The observed excitation-energy dependence (140 cm^{-1} eV^{-1}) of the 1833 cm^{-1} mode is in excellent agreement with the theoretical value of 139 cm^{-1} eV^{-1} of the $L_1 + D'$ mode.

The line width of the G mode in whiskers is slightly larger than that of the G mode in HOPG. The small line width of the Raman lines in whiskers indicates that the whisker has a very good crystal quality, which is indicated by the HRTEM image (figure 6*b*) and electron diffraction pattern (figure 6*e*) of graphite whiskers. The observation of the high-order Raman modes is limited by the crystalline quality. With 488.0 nm excitation, higher-order Raman modes up to fifth-order mode at 7478 cm^{-1} have been observed in the Raman spectra of whiskers, whose assignments are marked out in figure 8. These high-order Raman modes in whiskers have narrower peak widths and have much stronger intensities relative to the G mode than those of other carbon materials, such as HOPG, PG and carbon nanotubes (Kawashima & Katagiri 1995; Tan *et al*. 1999). This indicates that graphite has a high degree of crystalline order. There is no doubt that the high crystalline quality of whiskers and the strong enhancement of the D and 2D modes are helpful to the observation of such high-order Raman modes in the whiskers.

In addition to the intensity enhancement and narrow peak width, the L_1, L_2 and D modes in whiskers exhibit an asymmetric profile. Their Stokes and anti-Stokes components cannot be fitted with a single Lorentzian line shape (Tan *et al*. 2002), as shown in figure 9. Based on the inter-valley and intra-valley DR mechanisms (Cançado *et al*. 2002; Tan *et al*. 2002), the first-order dispersive mode can be decomposed into two peaks that are not associated with resonances with the incident and scattered photons, but rather are related to whether the first scattering event is by a phonon or by a defect. Considering this fact, we use two Lorentzian peaks at ω_- and ω_0 to fit the Stokes component of these modes, and two Lorentzian peaks at ω_0 and ω_+ to fit their anti-Stokes components, respectively, where ω_-, ω_0 and ω_+ are the phonon frequencies corresponding to three different phonon wave vectors determined

by the DR Raman processes of these dispersive modes (Tan *et al.* 2002). In the fitting process, three Lorentzian peaks at ω_-, ω_0 and ω_+ keep almost the same peak widths, but their intensities are adjustable to better fit the asymmetric profile of the first-order dispersive mode at Stokes and anti-Stokes sides. The Stokes and anti-Stokes sides of dispersive modes can be fitted well by two Lorentzian peaks, separated by a frequency equal to the observed frequency discrepancy between the Stokes and anti-Stokes components of a dispersive mode (Tan *et al.* 2002). It should be pointed out that a first-order dispersive mode does not always contain two Lorentzian peaks with equal intensity like the L_2 mode. If the mode is much broadened or one of the two Lorentzian peaks dominates the dispersive mode, it can be fitted well by only one Lorentzian peak. For the overtone of a dispersive mode, its Stokes and anti-Stokes Raman lines, however, are located at $2\omega_-$ and $2\omega_+$, respectively, and exhibit a single Lorentzian line shape (Cançado *et al.* 2002; Tan *et al.* 2002).

Like the D mode, the intensity of the D′ mode is directly correlated with the degree of disorder in carbon materials (Katagiri *et al.* 1988; Tan *et al.* 1998, 2001). The D′ mode appears close to 1624 cm^{-1} as a weak shoulder of the G mode in the observed Raman spectra of ion-implanted HOPG and microcrystalline graphite. However, the D′ mode frequency in graphite whiskers changes from 1623 cm^{-1} for the blue excitation to 1618 cm^{-1} for the red excitation; the excitation energy's dependence on the D′ mode frequency is *ca.* 10 cm^{-1} eV^{-1} in this range, and its frequency discrepancy of the Stokes and anti-Stokes components is 4 cm^{-1} for the red excitation (Tan *et al.* 2001). Similar results are also observed in Raman spectra of multi-walled carbon nanotubes (Tan *et al.* 2002) and graphite crystal edge planes (figure 3*a*). The excitation-energy dependence of the D′ mode frequency is attributed to the phonon wave vector selectivity for different excitations resulting from the DR Raman effect (Tan *et al.* 2002). The D′ mode frequency variation in different graphite materials with the same excitation results from a small modification of their phonon dispersion relations due to the slight changes of their atomic structures.

The Stokes and anti-Stokes Raman scattering of the first- and second-order dispersive modes of graphite whisker (Tan *et al.* 2001) clearly shows that the frequency discrepancy between the Stokes and anti-Stokes sides of a Raman mode in graphite materials is determined by a product of $\hbar\omega$ and $\partial\omega/\partial\varepsilon_{\mathrm{laser}}$, where ω is the Stokes frequency of the Raman mode. The frequency difference of an overtone in the Stokes and anti-Stokes spectra is found to be about four times as large as that of its fundamental mode (Tan *et al.* 1998, 2001), which can be understood by the DR Raman scattering mechanism (Cançado *et al.* 2002; Tan *et al.* 2002).

Figure 10*a* shows the polarized Raman spectra of a graphite whisker measured for the VV and HV scattering configurations when the axis of the graphite whisker was aligned perpendicular to the polarization of the scattered light as shown in the inset. The relative intensity of the Raman signal for the VV configuration to that for the HV configuration is usually defined as the depolarization ratio (Tan *et al.* 2001)

$$\rho(\varphi,\theta) = I_{\mathrm{VV}}(\varphi,\theta)/I_{\mathrm{HV}}(\varphi,\theta), \tag{3.1}$$

where φ is the angle (67.5°) between the graphite layers and the whisker axis and θ is the oriented angle of the whisker axis with respect to the $\hat{y}$-axis (in the (y,z)-plane) (figure 10 inset). For the scattering configuration ($\theta = 90°$) in figure 10, the depolarization ratio of the G mode, $\rho_{\mathrm{G}}(\varphi, 90°)$, is equal to $1/\cos^2(\varphi)$ and the calculated ratio of 6.8 is very close to the experimental value (5.8). The interesting

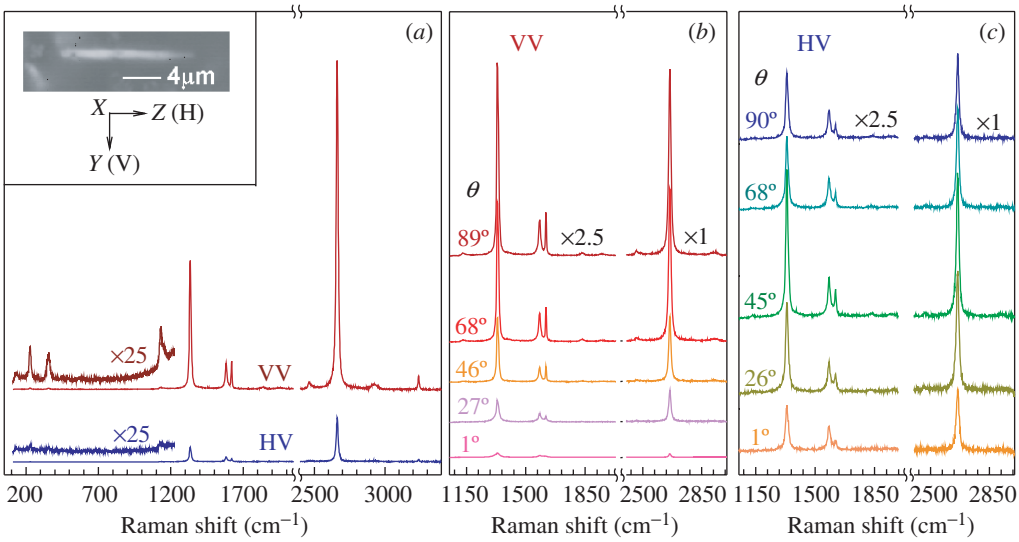

Figure 10. (*a*) Raman spectra of a graphite whisker in the VV and HV scattering configurations, while the whisker axis is aligned perpendicular to the polarization of the scattered light. The inset shows the optical micro-image of the measured whisker and the set of the Cartesian coordinate system. Angular dependence of the peak intensities of the D, G, D′ and 2D modes in the (*b*) VV and (*c*) HV configurations.

result is that the depolarization ratios of the D and D′ modes and their overtones 2D and 2D′ modes are 9.0, 10.0, 7.6 and 6.0, respectively, which are larger than that of the G mode with E_{2g} symmetry. The high depolarization ratios of the L_1 (8.1) and L_2 (9.2) modes also confirm that they are intrinsic modes of the whiskers rather than modes arising from impurities. The intensities of the G, D and D′ modes and their overtones (the 2D and 2D′ modes) in the VV and HV configurations were measured in detail for different angles (θ) between the polarizations of the scattered light and the whisker axis, as shown in figure 10*b*, *c*. For the VV configuration, all the Raman modes show a maximum intensity when the polarization of the incident laser light is perpendicular to the whisker axis ($\theta = 90°$), while near $\theta = 0°$ all the Raman modes reach a minimum intensity. However, for the HV configuration, all the Raman modes showed a minimum intensity when the polarization of the incident laser light is perpendicular or parallel to the whisker axis ($\theta = 90°$ or $0°$), while near the axis $\theta = 45°$ the intensity of all the Raman modes reaches a maximum value. The calculated orientation dependence of the tensor elements of the E_{2g} mode is in agreement with the experimental results (Tan *et al.* 2001). The small discrepancy between the theoretical and experimental results is a result of mixed character of non-centre phonon modes in the BZ of graphite and the resonant Raman effect.

4. Raman scattering of a tubular graphite cone

Recently, so-called tubular graphite cones (TGCs) were synthesized on an iron needle using the chemical vapour deposition method (Zhang *et al.* 2003). TGCs can potentially be used as tips for scanning probe microscopy because of the greater rigidity and easier mounting than the carbon nanotubes currently used. The cones

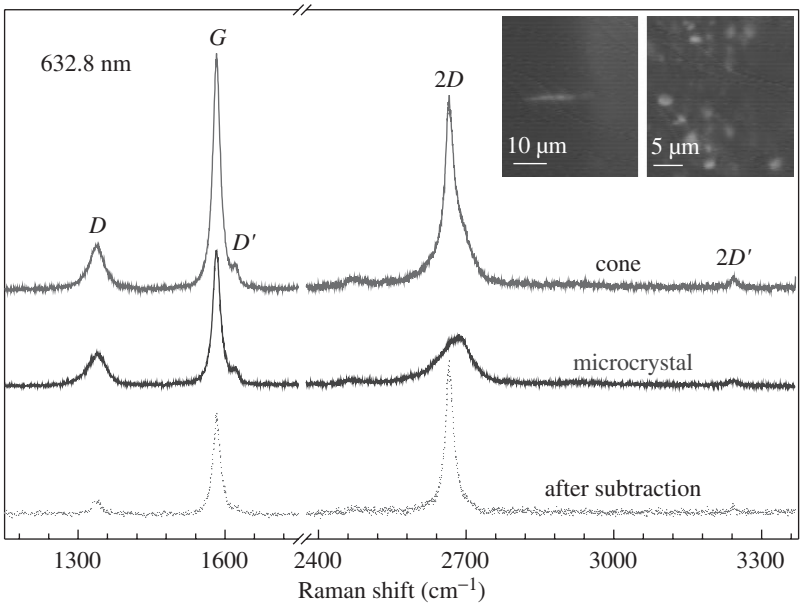

Figure 11. Raman scattering of a TGC and a GM in the as-grown sample. The insets show the optical micro-images of TGCs and GMs. The dotted line shows the spectrum of the TGC subtracted from that of the GM.

have nanometre-sized tips, micrometre-sized roots and hollow interiors with a diameter ranging from about two to several tens of nanometres. The cones are composed of cylindrical graphite sheets; a continuous shortening of the graphite layers from the interior to the exterior makes them cone-shaped. All of the TGCs have a faceted morphology. Their structural properties and SEM, TEM and electron diffraction patterns can be found in Zhang *et al*. (2003).

The insets in figure 11 show optical images of the measured iron needle, where an individual TGC can be clearly identified and easily relocated. Many graphite microcrystals (GMs) were also found on the surface of iron needles, whose optical micro-images are shown in the right inset of figure 11. Raman scatterings from the individual TGC and a GM excited by a 632.8 nm laser are shown in figure 11. The Raman spectrum of the GM is similar to that of (ion-implanted) HOPG with the same excitation (Tan *et al*. 1998), such as a doublet spectral structure and a lower intensity of the 2D mode relative to the G mode. The Raman spectrum of the TGC shows, however, some unusual spectral features. The equal line width of 18 cm^{-1} for the G mode in the TGC, the GM and graphite whisker indicates that TGC has a high crystal quality. The 2D mode in TGC shows an asymmetric line shape with a sharp peak at *ca.* 2665 cm^{-1}. This peak also has a shoulder at its high- and low-energy sides, whose line shape is very similar to that of the broad 2D peak of the GM. The Raman spectrum of the TGC subtracted from that of the GM is shown as the dotted line in figure 11. The fitted line widths of the D, G, D′, 2D and 2D′ modes in the remnant spectrum are 18, 18, 9, 20 and 9 cm^{-1}, respectively, which are very close to those in graphite whiskers (Tan *et al*. 2001). The D mode in the remnant spectrum can be well fitted by two peaks at *ca.* 1332 and 1342 cm^{-1}; the frequency of the 2D mode is just twice that of the D mode at 1332 cm^{-1}. This further confirms the

doublet behaviour of the first-order dispersive modes in carbon materials (Cançado *et al*. 2002; Tan *et al*. 2002).

The above analysis reveals that the Raman spectrum of the TGC is composed of two parts: one is similar to the spectrum of GMs and the other is similar to that of graphite whiskers. According to the size of the TGCs and the spot size (*ca*. 1 μm) of the excitation laser, all the Raman signals are from the individual TGC. The HRTEM image shows that TGCs have a well-ordered graphitic structure with an inner interlayer spacing of *ca*. 0.34 nm. Therefore, the GM-like spectral component of the TGC is from carbon layers beyond the surface of TGCs, and the whisker-like spectral component (dotted line in figure 11) originates from several carbon layers with frill-like bent structures close to the surface of the TGCs. Because the average tip apex angle of the TGC is 6–7° and defects, or disorder, may exist within one layer, fewer bending layers can be involved in the coherent coupling of the electronic states between the neighbouring carbon layers close to the surface of the TGC. As a result, the intensity enhancement of the 2D mode to the G mode is much weaker than that in whiskers.

5. Raman scattering from graphite polyhedral crystals

Polyhedral nano- and microstructures which typically have shapes of faceted rods or double-tipped pyramids, called graphite polyhedral crystals (GPCs), were recently found in pores of glassy carbon (Gogotsi *et al*. 2000). They have nanotube cores and graphite faces, which exhibit unusual sevenfold, ninefold or more complex axial symmetry (figure 12). Some of them are large, radially extended polygonized nanotubes. The crystals are up to 1 μm in cross-section, and 5 μm in length and can probably be grown in larger sizes.

The regular shape of many GPCs (figure 12*a*) suggests that the folding of the carbon cylinders was not stochastic, and rather that it followed certain crystallographic principles (fixed angles and/or number of facets). Formation of semitoroidal features at the terminations of layers (marked with arrow 2 in figure 12*c*) has been reported for nanotubes (Dresselhaus *et al*. 1996). A very large number (figure 12*b*) of ordered carbon layers (up to 1500) growing on a nanotube core results in complex axial symmetries of these structures. The crystal habits of the GPCs are based on the molecular symmetry of their nanotube cores, which are known to have variable screw-axis structure.

The size and aspect ratio of GPCs enabled acquisition of Raman spectra from the individual crystals. Submicrometre-sized GPCs are highly graphitized structures with the extinct D band and the G band of about the same width (FWHM = 14 cm^{-1}) as in the crystals of natural graphite (Ray & McCreery 1997). This can be explained by a smaller number of terminated graphene planes in GPC compared with a graphite crystal of the same size. The largest crystals were sufficient in size to enable selective micro-Raman analysis (figure 13) from the side face and the tip. Spectra from the crystal faces correspond to perfect graphite with a narrow G band and no D band, as expected from the TEM analysis of GPC faces (figure 12*b*). Spectra from the tips feature an unusually strong 2D (2706 cm^{-1}) overtone that exceeds the intensity of the G band in graphite. It is similar to the spectra of graphite whiskers (figure 7) but slightly weaker. The featured spectrum in figure 13 shows the strongest 2D band that we recorded for GPC. Again, similar to whiskers,

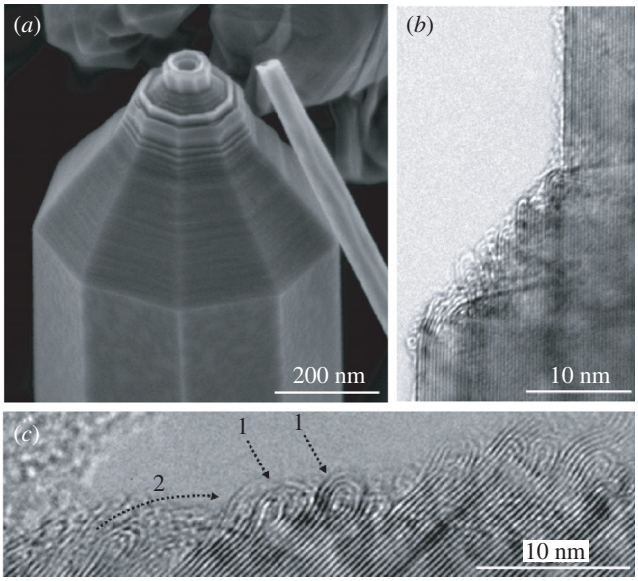

Figure 12. Graphite polyhedral crystals: (*a*) SEM micrograph of a nine-facet axial GPC; (*b*) and (*c*) TEM micrographs from the pyramidal region of a GPC show a large number of graphitic layers (*b*), and zipping of the layer ends into loops (1) forming a semitoroidal structure (2) within the tip region (*c*).

two additional bands were observed in the second-order frequency range at *ca.* 1895 and 2045 cm^{-1} (figure 13).

A number of weak low-frequency bands were observed in the initial study of GPCs, including a doublet at 184/192 cm^{-1} (Gogotsi *et al.* 2000), which is in good agreement with spectra from single-wall nanotubes (Rao *et al.* 1997). Such a spectrum could result if all of the dangling bonds were eliminated by the formation of closed graphitic layers, as shown in the TEM insets in figure 12*b*, *c*. Typically, a loop is built by 2–6 adjacent graphitic layers. The radius of curvature of the outer layer is similar to the average radius of double-walled nanotubes (Ci *et al.* 2003). Similar structural features were observed to form by elimination of dangling bonds after annealing of cup-like multi-walled nanotubes at 1500 °C (Endo *et al.* 2003); however, no low-frequency bands were reported in Endo's work. Well-defined curved termination of graphite sheets (Rotkin & Gogotsi 2002) have also been reported for a number of other carbon structures. These modes may also be acoustic modes, similar to the L_1 mode of whiskers (figure 7). The mode dependency on the excitation energy was not measured, since finding the same GPCs after switching the laser was not a trivial issue. Similar low-frequency bands were observed in the spectra from the graphite crystal edges (figure 4).

Several bands were also observed in the range 1440–1500 cm^{-1} (figures 13 and 14*a*). The positions of those bands vary from crystal to crystal and may reflect variations in the GPC structure. Two new bands were also observed in the second-order spectra at *ca.* 3151 and *ca.* 3174 cm^{-1} (figure 14*b*). Unlike the 1440–1500 cm^{-1} lines, the positions of these modes have fixed values; the assignment of these modes is not known.

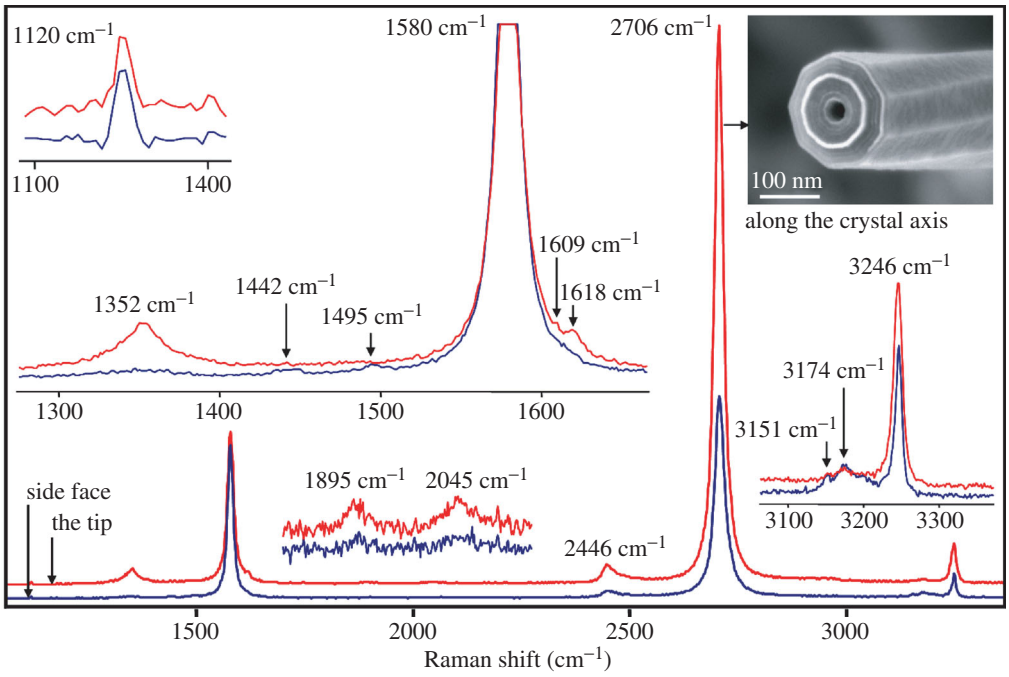

Figure 13. Fundamental, combination modes and overtones in Raman spectra taken from the side face and the tip of an individual graphite polyhedral crystal (514.5 nm excitation).

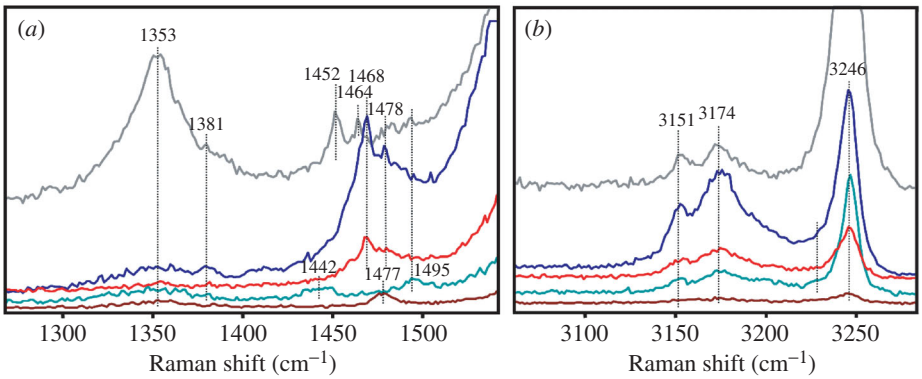

Figure 14. Raman scattering from graphite polyhedral crystals: (*a*) 1400–1500 cm^{-1} lines, and (*b*) 3151 and 3174 cm^{-1} features (514.5 nm excitation).

When discussing Raman spectra from a single GPC, it is necessary to take into account the fact that the crystals are very poorly resolved under the light microscope. Therefore, it is not possible to give a detailed correlation between the Raman spectra and the structural features of GPCs (helical or straight crystals, symmetric or not). Still, based on an analysis of the Raman spectra (narrow G band, no D band and almost perfect graphite second-order spectrum) and TEM, GPCs are closer to perfect than multi-walled nanotubes or cylindrical graphite whiskers, which always show a distinct D band.

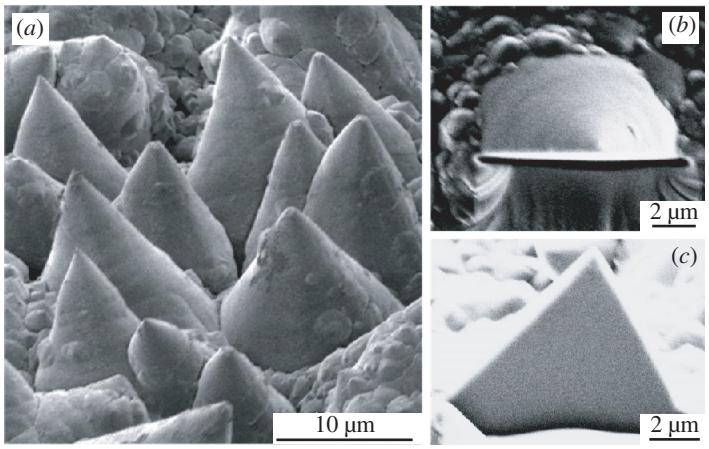

Figure 15. SEM micrographs of naturally occurring carbon cones; (*b*) and (*c*) show a cone cut in two parts using a focused ion beam (FIB). No cavity was observed inside the cone.

6. Raman scattering from natural carbon cones

The first occurrence of natural graphite cones (figure 15) was recently reported by Jaszczak *et al*. (2003). The cones were found on the surfaces of millimetre-sized polycrystalline spheroidal aggregates of graphite. Their heights ranged from less than 1 µm to 40 µm, which is larger than synthetic carbon cones reported in the literature, and, unlike most laboratory-produced cones, the natural cones have a wide distribution of apex angles, which supports a disclination model (Double & Hellawell 1974) for cone-helix structures.

Spheroidal and triskelial aggregates of graphite (0.1–10 mm in diameter) occur in calcite boudins up to 30 cm in diameter from the Bancroft shear zone (Van der Pluijm & Carlson 1989; Carlson *et al*. 1990) in the Central Metasedimentary Belt of the Canadian Grenville province, and are exposed at roadcuts 3–5 km south of Gooderham, Ontario, Canada (Jaszczak *et al*. 2003). Of over 1000 spheres and spheroids that have been examined, 12 have been observed to have clearly identifiable cones on their surfaces. The cones appear highly reflective with a silver-white metallic lustre. They are observed to dominate sample surfaces. The cones surface topography and petrologic relations suggest they formed from a hydrothermal fluid.

Raman microspectroscopy analysis of about 20 carbon cones showed very little variation with respect to the size or apex angle. Both the first- and second-order spectra of the cones (figure 16) were similar to those of microcrystalline graphite and of multi-walled nanotubes (Libera & Gogotsi 2001) with slightly upshifted D and G bands. Upshift of Raman bands from the positions typical for planar graphite (*ca*. 1355 and 1582 cm^{-1}, respectively) may be attributed to the curved cone surfaces and the confinement effect of phonon modes because of the smaller crystallite planar size in natural carbon cones. The presence of the D band in all spectra shows that the surfaces of the cones are not perfectly wrapped in a graphene sheet and the graphene planes terminate at the cone surface forming the growth steps seen in figure 6*b*, *d*. Broadening of the G band (*ca*. 34 cm^{-1} in cones compared with 14 cm^{-1} for a planar single crystal) can result from the conical wrapping of the layers and the bending of the graphene sheets. The intensity of the D band relative to the G band was lower

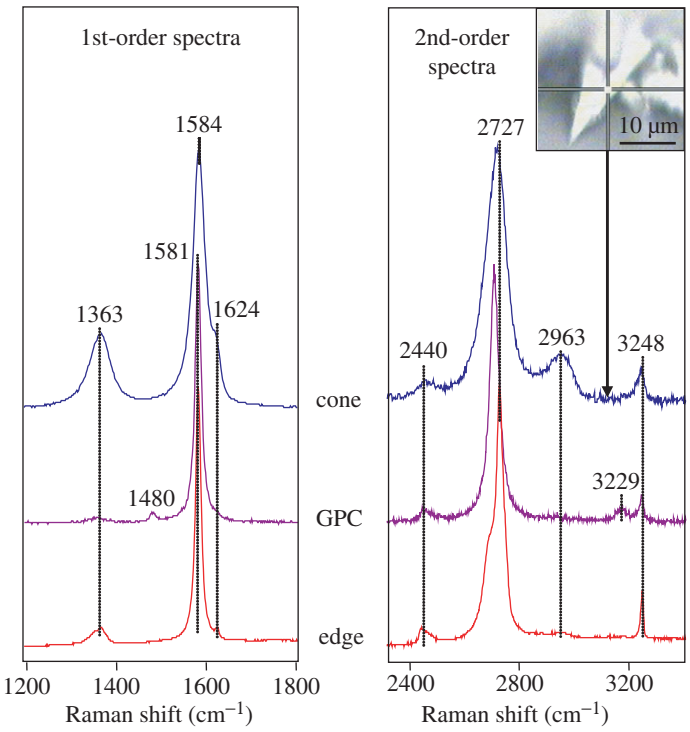

Figure 16. First- and second-order Raman spectrum of a naturally occurring carbon cone in comparison with Raman spectra of graphite edge planes and graphite polyhedral crystals (514.5 nm excitation).

compared with graphite whiskers (figures 7 and 8), which are assumed to be formed by the same disclination mechanism as the cones, but higher than in GPCs (Gogotsi *et al.* 2002). The second-order spectrum of the cones was also much weaker than that of GPCs or whiskers. In general, spectra of natural cones are similar to that of microcrystalline graphite.

7. Conclusion

Non-planar graphitic materials, such as arched edge planes of graphite crystals, graphite polyhedral crystals, TGCs, graphitic whiskers and carbon (nano)cones, produce Raman spectra that are, in most cases, distinctly different from those of planar graphite or disordered graphitic carbons. Unique spectral features, when compared with other carbon materials, include additional weak peaks, often at low frequencies, asymmetric shape or splitting of the D mode, and an intensity of the second-order peaks exceeding that of the first order. Anomalously strong peaks in the second-order spectra have been registered for graphite whiskers and polyhedral crystals. The 2D overtone in whiskers could be 13 times stronger than the first-order G mode. In graphite polyhedral crystals, the 2D overtone was observed to be two to three times stronger than the G mode. This enhancement may originate from the enhanced DR Raman process of dispersive modes due to the coupled coherent electronic states between the neighbouring carbon layers with frill-like bent structures near the sur-

face region of non-planar graphitic materials. The main feature in the Raman spectra from natural graphite crystal edge planes is the splitting of the D mode. This splitting is *ca.* 20 cm^{-1} and is different from the one observed for whiskers (9 cm^{-1}). Most of the observed new features can be explained by the DR Raman scattering mechanism. Raman spectroscopy provides useful information about the crystal quality, phonon and band structure of carbon materials and can be used for identification of non-planar graphitic structures.

The work at Drexel University was supported by the DOE grant DE-FJ02-01ER45932. The purchase of the Raman spectrometer and environmental SEM was supported by NSF grants DMR-0116645 and BES-0216343. S.D. and Y.G. are grateful to Professor John Jaszczak, Michigan Technological University, for providing the samples of planar and conical crystals of natural graphite for this study. We are also thankful to Dr V. Domnich, Mr J. A. Libera and Mr K. Behler for experimental assistance and comments on the manuscript. P.T. acknowledges the support of the special funds for Major State Basic Research Project no. G001CB3095 of China and thanks Professor WanCi Shen, Professor EnGe Wang, Dr Jian Dong and Dr GuangYu Zhang for providing the samples (graphite whiskers and TGCs) for this study.

Appendix A. Experimental details

The samples were analysed using a Philips XL 30 environmental field-emission SEM. SEM analysis was always accompanied by EDS analysis to verify that the analysed material was carbon. TEM analysis was performed using a JEOL JEM-2010F (200 kV). A Gatan image filter for energy filtered imaging and electron energy loss spectroscopy was used to identify carbon areas and impurities. TEM samples were prepared by dispersing the synthesis products in isopropyl alcohol over a copper grid with a lacey carbon film. Raman microspectroscopy (Renishaw 1000 or Dilor Super Labram) with the excitation wavelengths of 488.0 nm (blue line of an Ar^+ laser), 514.5 nm (green line of an Ar^+ laser), 633 nm (He–Ne laser) and 780 nm (diode laser) was used to analyse the samples. The spectra were collected from a spot size of 1–2 μm. Low laser power was applied to avoid damaging and heating the sample. Spectral analysis software GRAMS 32 v. 5.2 was used for peak fitting and deconvolution.

References

Bacon, R. 1960 Growth, structure, and properties of graphite whiskers. *J. Appl. Phys.* **31**, 283–290.

Bowling, R. J., Packard, R. T. & McCreery, R. L. 1989 Activation of highly ordered pyrolytic graphite for heterogeneous electron transfer: relationship between electrochemical performance and carbon microstructure. *J. Am. Chem. Soc.* **111**, 1217–1223.

Brar, V. W., Samsonidze, Ge. G., Dresselhaus, M. S., Dresselhaus, G., Saito, R., Swan, A. K., Ünlü, M. S., Goldberg, B. B., Souza Filho, A. G. & Jorio, A. 2002 Second-order harmonic and combination modes in graphite, single-wall carbon nanotube bundles, and isolated single-wall carbon nanotubes. *Phys. Rev.* B **66**, 155418.

Cançado, L. G., Pimenta, M. A., Saito, R., Jorio, A., Ladeira, L. O., Grueneis, A., Souza Filho, A. G., Dresselhaus, G. & Dresselhaus, M. S. 2002 Stokes and anti-Stokes double resonance Raman scattering in two-dimensional graphite. *Phys. Rev.* B **66**, 035415.

Carlson, K. A., Van der Pluijm, B. A. & Hanmer, S. 1990 Marble mylonites of the Bancroft shear zone: evidence for extension in the Canadian Grenville. *Geol. Soc. Am. Bull.* **102**, 174–181.

Ci, L. J. (and 11 others) 2003 Temperature dependence of resonant Raman scattering in double-wall carbon nanotubes. *Appl. Phys. Lett.* **82**, 3098–4000.

Compagnini, G., Puglisi, O. & Foti, G. 1997 Raman spectra of virgin and damaged graphite edge planes. *Carbon* **35**, 1793–1797.

Dillon, R. O., Woolam, A. & Katkanant, V. 1984 Use of Raman scattering to investigate disorder and crystallite formation in as-deposited and annealed carbon films. *Phys. Rev.* B **29**, 3482–3489.

Dimovski, S., Libera, J. A. & Gogotsi, Y. 2002 A novel class of carbon nanocones. *Mater. Res. Soc. Symp. Proc.* **706**, Z6.27.1–Z6.27.6.

Dimovski, S., Jaszczak, J. A., Robinson, G. W., Gogotsi, Y. & Hackney, S. A. 2004 Naturally occurring cones and tubes of graphite. In *Carbon 2004 Conf. Proc., 11–16 July 2004, Providence, RI, USA*. Madison, WI: Omnipress. (In the press.)

Dong, J., Shen, W. C., Zhang, B. F., Liu, X., Kang, F. Y., Gu, J. L., Li, D. S. & Chen, N. P. 2001 New origin of spirals and new growth process of carbon whiskers. *Carbon* **39**, 2325–2333.

Dong, J., Shen, W. C., Kang, F. Y. & Tatarchuk, B. 2003 Whiskers with apex angle 135 degree growing by a disclination growth mechanism. *J. Cryst. Growth* **245**, 77–83.

Double, D. D. & Hellawell, A. 1974 Cone-helix growth forms of graphite. *Acta Metall.* **22**, 481–487.

Dresselhaus, M. S., Dresselhaus, G. & Eklund, P. C. 1996 *Science of fullerenes and carbon nanotubes*. Academic.

Dresselhaus, M. S., Dresselhaus, G., Pimenta, M. A. & Eklund, P. C. 1999 Raman scattering in carbon materials. In *Analytical applications of Raman spectroscopy* (ed. M. J. Pelletier). Oxford: Blackwell Science.

Endo, M., Lee, B. J., Kim, Y. A., Muramatsu, H., Yanagisawa, T., Hayashi, T., Terrones, M. & Dresselhaus, M. S. 2003 Transitional behaviour in the transformation from active end planes to stable loops caused by annealing. *New J. Phys.* **5**, 121.

Ferrari, A. C. & Robertson, J. 2000 Interpretation of Raman spectra of disordered and amorphous carbon. *Phys. Rev.* B **61**(20), 14 095–14 107.

Gogotsi, Y., Libera, J. A., Kalashnikov, N. & Yoshimura, M. 2000 Graphite polyhedral crystals. *Science* **290**, 317–320.

Gogotsi, Y., Dimovski, S. & Libera, J. A. 2002 Conical crystals of graphite. *Carbon* **40**(12), 2263–2284.

Grüneis, A., Saito, R., Kimura, T., Cançado, L. G., Pimenta, M. A., Jorio, A., Souza Filho, A. G., Dresselhaus, G. & Dresselhaus, M. S. 2002 Determination of two-dimensional phonon dispersion relation of graphite by Raman spectroscopy. *Phys. Rev.* B **65**, 155405.

Haanstra, H. B., Knippenberg, W. F. & Verspui, G. 1972 Columnar growth of carbon. *J. Cryst. Growth* **16**, 71–79.

Jaszczak, J. A. 1995 Graphite: flat, fibrous and spherical. In *Mesomolecules: from molecules to materials* (ed. G. D. Mendenhall, A. Greenberg & J. F. Liebman), pp. 161–180. London: Chapman and Hall.

Jaszczak, J. A., Robinson, G. W., Dimovski, S. & Gogotsi, Y. 2003 Naturally occurring graphite cones. *Carbon* **41**, 2085–2092.

Katagiri, G., Ishida, H. & Ishitani, A. 1988 Raman spectra of graphite edge planes. *Carbon* **26**(4), 565–571.

Kawashima, Y. & Katagiri, G. 1995 Fundamentals, overtones, and combinations in the Raman spectrum of graphite. *Phys. Rev.* B **52**, 10 053–10 059.

Kawashima, Y. & Katagiri, G. 1999 Observation of the out-of-plane mode in the Raman scattering from the graphite edge plane. *Phys. Rev.* B **59**, 62–64.

Lespade, P., Al-Jishi, R. & Dresselhaus, M. S. 1982 Model for Raman scattering from incompletely graphitized carbons. *Carbon* **20**(5), 427–431.

Libera, J. A. & Gogotsi, Y. 2001 Hydrothermal synthesis of graphite tubes using Ni catalyst. *Carbon* **39**(9), 1307–1318.

Minkoff, I. 1986 *Solidification and cast structure*, pp. 42–47. Wiley.

Murayama, H. & Maeda, M. 1990 A novel form of filamentous graphite. *Nature* **345**(28), 791–793.

Nemanich, R. J. & Solin, S. A. 1979 First- and second-order Raman scattering from finite-size crystals of graphite. *Phys. Rev.* B **20**, 392–401.

Nemanich, R. J., Lucovsky, G. & Solin, S. A. 1977 Optical probes of the lattice dynamics of graphite. *Mater. Sci. Engng* **31**, 157–160.

Nemanich, R. J., Glass, J. T., Lucovsky, G. & Shroder, R. E. 1988 Raman-scattering characterization of carbon bonding in diamond and diamondlike thin-films. *J. Vac. Sci. Technol.* A **6**, 1783–1787.

Nicklow, R., Wakabayashi, N. & Smith, H. G. 1972 Lattice dynamics of pyrolytic graphite. *Phys. Rev.* B **5**(12), 4951–4962.

Rao, A. M. (and 12 others) 1997 Diameter-selective Raman scattering from vibrational modes in carbon nanotubes. *Science* **275**, 187–191.

Ray, K. & McCreery, R. L. 1997 Spatially resolved Raman spectroscopy of carbon electrode surfaces: observations of structural and chemical heterogeneity. *Analyt. Chem.* **69**, 4680–4687.

Rotkin, S. V. & Gogotsi, Y. 2002 Analysis of non-planar graphitic structures: from arched edge planes of graphite crystals to nanotubes. *Mater. Res. Innovat.* **5**, 191–200.

Saito, R., Jorio, A., Souza Filho, A. G., Dresselhaus, G., Dresselhaus, M. S. & Pimenta, M. A. 2002 Probing phonon dispersion relations of graphite by double resonance Raman scattering. *Phys. Rev. Lett.* **88**, 027401.

Tan, P. H., Deng, Y. M. & Zhao, Q. 1998 Temperature-dependent Raman spectra and anomalous Raman phenomenon of highly oriented pyrolytic graphite. *Phys. Rev.* B **58**, 5435–5439.

Tan, P. H., Tang, Y., Deng, Y. M., Li, F., Wei, Y. L. & Cheng, H. M. 1999 Resonantly enhanced Raman scattering and high-order Raman spectra of single-walled carbon nanotubes. *Appl. Phys. Lett.* **75**, 1524–1527.

Tan, P. H., Hu, C. Y., Dong, J., Shen, W. C. & Zhang, B. F. 2001 Polarization properties, high-order Raman spectra, and frequency asymmetry between Stokes and anti-Stokes scattering of Raman modes in a graphite whisker. *Phys. Rev.* B **64**, 214301.

Tan, P. H., An, L., Liu, L. Q., Guo, Z. X., Czerw, R., Carroll, D. L., Ajayan, P. M., Zhang, N. & Guo, H. L. 2002 Probing the phonon dispersion relations of graphite from the double resonance processes of Stokes and anti-Stokes Raman scatterings in multi-walled carbon nanotubes. *Phys. Rev.* B **66**, 245410.

Tan, P. H., Zhang, G. Y. & Wang, E. G. 2004 Raman spectra from an individual tubular graphite cone. (Submitted.)

Thomsen, C. & Reich, S. 2000 Double resonant Raman scattering in graphite. *Phys. Rev. Lett.* **85**, 5214–5217.

Tsuzuku, T. 1957 Conical spiral structure and laminar cleavage of graphite. *J. Phys. Soc. Jpn* **12**, 778–788.

Tuinstra, F. & Koenig, J. L. 1970 Raman spectrum of graphite. *J. Chem. Phys.* **53**(3), 1126–1130.

Van der Pluijm, B. A. & Carlson, K. A. 1989 Extension in the central metasedimentary belt of the Ontario Grenville: timing and tectonic significance. *Geology* **17**, 161–164.

Vidano, R. & Fischbach, D. B. 1978 New lines in the Raman spectra of carbons and graphite. *J. Am. Ceram. Soc.* **61**, 13–17.

Zhang, G. Y., Jiang, X. & Wang, E. G. 2003 Tubular graphite cones. *Science* **300**, 472–474.